Actin-dependent rapid recruitment of reluctant synaptic vesicles into a fast-releasing vesicle pool

Jae Sung Lee[a,b,c], Won-Kyung Ho[a,b,c], and Suk-Ho Lee[a,b,c,1]

[a]Cell Physiology Laboratory, Department of Physiology and [b]bioMembrane Plasticity Research Center, Seoul National University College of Medicine, Jongno-gu, Seoul 110-799, Republic of Korea; and [c]Neuroscience Research Institute, Seoul National University Medical Research Center, Jongno-gu, Seoul 110-799, Republic of Korea

Edited* by Erwin Neher, Max-Planck Institute for Biophysical Chemistry Goettingen, Germany, and approved February 9, 2012 (received for review August 27, 2011)

Glutamatergic synaptic terminals harbor reluctant synaptic vesicles (SVs) that contribute little to synchronous release during action potentials but are release competent when stimulated by sucrose or by direct intracellular application of calcium. It has been noted that the proximity of a release-competent SV to the calcium source is one of the primary factors that differentiate reluctant SVs from fast-releasing ones at the calyx of Held synapse. It has not been known whether reluctant SVs can be converted into fast-releasing ones. Here we show that reluctant SVs are recruited rapidly in an actin-dependent manner to become fast-releasing SVs once the pool of fast-releasing SVs is depleted by a short depolarization. Recovery of the pool of fast-releasing SVs was accompanied by a parallel reduction in the number of reluctant SVs. Quantitative analysis of the time course of depletion of fast-releasing SVs during high-frequency stimulation revealed that in the early phase of stimulation reluctant SVs are converted rapidly into fast-releasing ones, thereby counteracting short-term depression. During the late phase, however, after reluctant vesicles have been used up, another process of calmodulin-dependent recruitment of fast-releasing SVs is activated. These results document that reluctant SVs have a role in short-term plasticity and support the hypothesis of positional priming, which posits that reluctant vesicles are converted into fast-releasing ones via relocation closer to Ca^{2+}-channels.

readily releasable pool | synaptic vesicle dynamics

Synaptic strength is determined by quantal size, the number of release-competent synaptic vesicles (SVs), and their release probability (Pr). The estimate for the number of release-competent SVs, which also is referred to as the "readily releasable pool (RRP) size," depends heavily on the method used for its determination. The RRP size estimated by a cumulative plot of the excitatory postsynaptic currents (EPSC) amplitudes evoked by high-frequency afferent fiber stimulation (RRP_{cum}) is smaller than that estimated by the application of a hypertonic sucrose solution or presynaptic strong depolarization (1–3). This discrepancy reflects the presence of reluctant SVs, which are scarcely released by an action potential (AP) at glutamatergic synaptic terminals. Consistently, deconvolution analysis of EPSCs evoked by a long depolarizing pulse at the calyx of Held revealed that release-competent SVs can be separated into fast- and slow-releasing SV pools (FRP and SRP, respectively) (4). The FRP vesicles are responsible for phasic release during a high-frequency train of action potentials (APs), whereas the SRP vesicles contribute primarily to asynchronous release, when the intracellular concentration of calcium ions ($[Ca^{2+}]$) is increased globally during the late period of the train (2). Thus, SRP vesicles can be regarded largely as reluctant SVs at the calyx of Held.

Despite the evidence for the presence of reluctant SVs at glutamatergic synapses, their role in short-term plasticity is not well understood. It has been demonstrated that SVs in the FRP and SRP show little difference in their Ca^{2+} sensitivity for fusion when stimulated by caged Ca^{2+}, suggesting that the proximity of a release-competent SV to the calcium source is one of the primary factors that determine its release kinetics (5), together with its intrinsic Ca^{2+} sensitivity (6). Based on this notion, it has been hypothesized that the conversion of slow-releasing SVs into fast-releasing SVs may involve the movement of SVs closer to Ca^{2+} sources (the positional priming hypothesis) (7), but this idea remains to be proven. Recently, we reported that calmodulin (CaM)-dependent posttetanic activation of myosin light-chain kinase (MLCK) increased the proportion of FRP to SRP, with the size of the total pool of release-competent SVs remaining constant (8). This result suggests that the FRP and SRP are in a dynamic equilibrium, regulated by MLCK-dependent activation of myosin II. In the present study, we inquired whether SRP vesicles can be recruited into the FRP. To address this question, we applied short depolarizing pulses that induced preferential depletion of the FRP with little effect on the SRP. We show that after such pulses the SRP size decreases in an actin-dependent manner, whereas the FRP recovers rapidly. Our results support the idea that SRP vesicles can be converted rapidly into fast-releasing vesicles. Furthermore, we demonstrate the role of this conversion in short-term plasticity.

Results

Recovery of Rapidly Releasing Vesicles After a Predepleting Pulse Is Accelerated by Residual Slowly Releasing Vesicles. The release-competent SV pool, identified by a long depolarizing pulse at the calyx of Held, can be separated into the FRP and SRP when 0.5 mM EGTA is included in the presynaptic pipette (4). Under experimental conditions similar to those of Sakaba and Neher (4), we investigated the recovery of the FRP using paired-pulse stimulation. To induce different degrees of SRP depletion under control conditions, the duration of the first pulse (the predepleting pulse, preDP) was varied from 3–50 ms (−80 to 0 mV preceded by a short episode to +70 mV for 2 ms). At a fixed interstimulus interval (ISI) of 750 ms, a second depleting pulse (0 mV for 30 ms, DP30) was applied to estimate the recovered fraction of the FRP. The experiments were performed in the presence of 100 μM cyclothiazide and 2 mM γ-D-glutamylglycine (γ-DGG) to reduce the effects of postsynaptic receptor desensitization and saturation. Examples of pre- and postsynaptic responses to predepleting pulses (*Left*) and second pulses (*Right*) are shown in Fig. 1*A*. The corresponding presynaptic release rates, estimated by deconvolution analysis, are shown in Fig. 1*B*. The recovered FRP fraction decreased as the preDP duration increased from 3 to 10 ms, whereas further increases of the preDP duration from 10 to 30 ms facilitated FRP recovery (Fig. 1*C*, *i*). The facilitation of FRP recovery by

Author contributions: J.S.L., W.-K.H., and S.-H.L. designed research; J.S.L. performed research; J.S.L. and S.-H.L. analyzed data; and J.S.L., W.-K.H., and S.-H.L. wrote the paper.

The authors declare no conflict of interest.

*This Direct Submission article had a prearranged editor.

[1]To whom correspondence should be addressed. E-mail: leesukho@snu.ac.kr.

See Author Summary on page 4728 (volume 109, number 13).

This article contains supporting information online at www.pnas.org/lookup/suppl/doi:10.1073/pnas.1114072109/-/DCSupplemental.

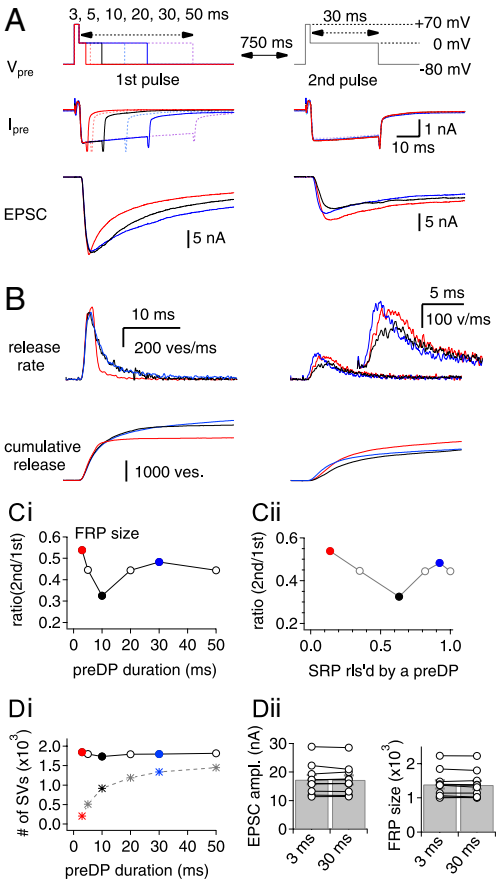

Fig. 1. The recovery of the FRP is facilitated by the remaining SVs in the SRP after a preDP. (*A*) Presynaptic dual-pulse protocol (V_{pre}; *Top*), resultant presynaptic Ca^{2+} current (I_{pre}; *Middle*), and EPSCs (*Bottom*). (*Left*) Pre- and postsynaptic responses evoked by preDPs of different durations are superimposed. (*Right*) The recovered fraction of FRP was estimated from the EPSC evoked by the second pulse applied after an ISI of 750 ms. All traces are depicted using the color code: preDP3, red; preDP10, black; preDP30, blue. EPSCs evoked by a preDP of 5, 20, and 50 ms are omitted for clarity. The dual-pulse protocol was applied every 40 s or longer. (*B*) Quantal release rate (*Upper*) and cumulative quantal release (*Lower*) estimated by the deconvolution analysis of EPSCs evoked by a preDP (*Left*) and by the second pulse (*Right*). (*C, i*) Recovered fraction of the FRP at an ISI of 750 ms as a function of the preDP duration. (*C, ii*) The recovered fraction of the FRP at the second pulse as a function of the fraction of SRP released by the first pulse (FRP_2/FRP_1). Note that the recovered fraction of the FRP was minimal at preDP 10 (black circle), and either shortening or lengthening the preDP duration from 10 ms led to enhancement of the FRP recovery. (*D, i*) Amounts of the FRP (circles) and SRP (asterisks) released by a preDP as a function of the preDP duration. (*D, ii*) Mean values for EPSC amplitude (*Left*) and FRP size (*Right*) evoked by a preDP of 3 or 30 ms. The results in *B–D, ii* were estimated from the raw data shown in *A* and are denoted by the color code used in *A*.

a preDP of longer duration has been shown in previous studies (4, 9) and is known as "Ca^{2+}-dependent recovery" (CDR). However, the inverse dependence of FRP recovery on the preDP duration between 3 and 10 ms had not yet been demonstrated. The recovered FRP fraction following the shortest preDP duration of 3 ms (preDP3) was 53.3 ± 2.1% (n = 10), which is significantly higher than that after a preDP of 10 ms duration (preDP10) (32.7 ± 1.9%, n = 10, $P < 0.01$). This result cannot be ascribed to an incomplete depletion of the FRP by a preDP3 because a preDP duration longer than 3 ms caused no further increases in FRP release but instead caused an increase in the released fraction of the SRP (Fig. 1*D*, *i*). No further increases in EPSC amplitude or in the FRP size by preDPs longer than 3 ms were confirmed in eight calyx synapses (Fig. 1*D*, *ii*). These results are consistent with a previous report (6).

We hypothesized that depletion of the SRP during longer preDPs might be responsible for the reduced FRP recovery when the preDP duration is between 3 and 10 ms. To assess the contribution of the SRP to the recovery of the FRP, we replotted the data of Fig. 1*C*, *i* against the corresponding fraction of the SRP released by the preDP (Fig. 1*C*, *ii*). For preDPs shorter than 10 ms, the recovered FRP at the second pulse exhibited an inverse relationship with the released fraction of the SRP, suggesting that the remaining SRP vesicles (or the residual SRP) may contribute to the recovery of the FRP. We refer to this mechanism as "SRP-dependent recovery of FRP size" (SDR). For longer preDPs, a different mechanism is activated (see below), which accelerates recruitment.

To test the concept of SDR further, we examined the size of the SRP at the second pulse after a preDP3. Because the SRP released by a preDP3 is minimal (9.0 ± 0.74%, n = 90 trials at 25 synapses) with the SRP being replenished rapidly (4), its size at the second pulse should be almost maximal. Contrary to this prediction, the SRP size estimated at 750 ms after a preDP3 was smaller (80.4 ± 2.2%, n = 10) than that expected for the case of no recovery, which typically was close to 90% (calculated by subtracting the SRP fraction released by a preDP3 from unity). Furthermore, the SRP size measured at an ISI of 200 ms was even smaller (73.4 ± 2.5%, n = 14) (Fig. S1*A*). These results suggest that the SRP is consumed for the recovery of the FRP. Taken together with the inverse dependence of FRP recovery on the size of the SRP released by a short preDP, our findings suggest that residual SVs remaining in the SRP after a preDP3 are recruited to the FRP.

Calmodulin-Dependent Mechanisms Underlie Ca^{2+}-Dependent Recovery but Not SRP-Dependent Recovery. The recovery of the FRP was enhanced as the duration of a preDP was increased further up to 30 ms (Fig. 1*C*, *i*). To test whether CDR is responsible for this effect, we performed experiments in the presence of a calmodulin inhibitor peptide (CaMip). Fig. 2*A* shows averaged traces of the first EPSC ($EPSC_1$, broken line) and the second EPSC ($EPSC_2$, solid line), normalized to the peak amplitude of $EPSC_1$. These ESPCs were evoked by a dual-pulse protocol with different preDP durations (columns in Fig. 2*A*) and under different presynaptic conditions (rows in Fig. 2*A*). For comparison, control traces for paired EPSCs are shown in black. When CaMip (20 μM) was included in the presynaptic pipette (red traces in Fig. 2*A* and red symbols in Fig. 2*B*; also see Table S1), the recovered FRP fraction was significantly lower than the control value after a preDP of 30 ms (preDP30) but not after a preDP10 or a preDP shorter than 10 ms. This result corroborates the distinction between CDR and SDR, because blocking calmodulin had no effect on SDR.

Polymerized Actin Is Required for both Forms of Vesicle Recruitment. It has been reported that actin filaments are abundant, intermixed with synaptic vesicles (10), and are present along the presynaptic membrane at the calyx of Held (11). Depolymerization of actin filaments suppresses the recovery of releasable SVs after depletion (12). Furthermore, we have reported that the posttetanic increase in the ratio of the FRP to SRP is abolished by inhibition of myosin ATPase (8). Therefore, we investigated the effect of actin disruption on the recovery of the FRP. Latrunculin B (latB; 15 μM), a specific inhibitor of actin polymerization, was applied through the presynaptic patch pipette. LatB suppressed both CDR (Fig. 2*A*, blue traces) and SDR (Fig. 2*B*, blue symbols) (also see Table S1), but it had no effect on the baseline recovery of the FRP observed after a preDP10 (31.2 ± 2.2%, n = 6, P = 0.63). We confirmed that the effects of latB on CDR and SDR are reversible in slices that were preincubated in artificial cerebrospinal fluid (aCSF) containing latB (Fig. S2). Next, we tested the involvement of myosin II, which was found to be colocalized with synaptophysin in the calyx terminal (Fig. S3). Similar to latB, blebbistatin

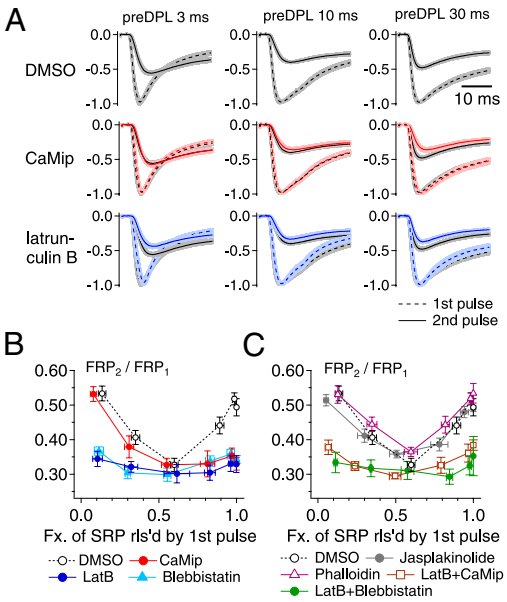

Fig. 2. The SDR of the FRP depends on polymerized actin filaments. (*A*) Averaged traces of the first and second EPSCs ($EPSC_1$ and $EPSC_2$) normalized to the peak amplitude of $EPSC_1$. Each row shows the normalized $EPSC_1$ (broken line) and $EPSC_2$ (solid line) evoked by a dual-pulse protocol (as shown in Fig. 1) with different preDP durations (*Left*, 3 ms; *Middle*, 10 ms; *Right*, 30 ms). Traces in each row were obtained with presynaptic treatment with the same drug: (*Top*) DMSO 1/1,000 as a control, $n = 10$; (*Middle*) 20 μM CaMip, $n = 7$; (*Bottom*) 15 μM latB, $n = 6$. Black traces in each panel represent the averaged EPSC traces evoked by the same pulse protocol under control conditions. Shading indicates the SE range of an averaged trace. (*B*) Mean values for the recovered fraction of the FRP at the second pulse (FRP_2/FRP_1) as a function of the fraction of SRP released by the first pulse under control conditions (open circles) or in the presence of CaMip (red circles), blebbistatin (light blue triangles), or latB (blue circles). (*C*) Mean values for the size of the recovered FRP (FRP_2/FRP_1) in the presence of jasplakinolide (gray circles), phalloidin (magenta triangles), latB plus CaMip (brown squares), or latB plus blebbistatin (green circles). The control values (open circles) are superimposed for comparison. Statistical values for recovered fractions after a preDP3, a preDP10, and a preDP30 under each condition are given in Table S1. Error bars indicate SEM.

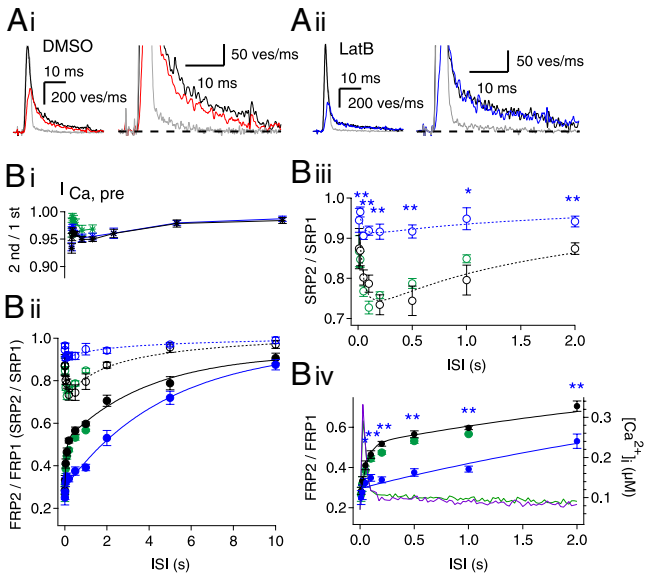

Fig. 3. Recovery time course of the FRP and concomitant change in the SRP size after a preDP3. (*A, i*) Representative quantal release estimated from EPSCs evoked by a naive DP30 (black trace) and a DP30 after a preDP3 (red trace) (ISI = 0.2 s; see also Fig. S1*A*). Note that the quantal release rate at the second pulse (red trace) is lower than the release rate for the naive pulse (black trace) in both the fast phase (*Left*) and the slow phase (*Right*; same traces as left in an expanded scale) under control condition. (*A, ii*) There is no difference in the naive pulse (black trace) and the DP30 after a preDP3 (blue trace) (ISI = 0.2 s; see also Fig. S1*B*). The gray trace in each panel represents a quantal release by a preDP3. (*B*) The ratio of the second amplitude to the first amplitude of the presynaptic Ca^{2+} current (*B, i*), and the sizes of the FRP (filled circles) and SRP (open circles) (*B, ii*) as a function of ISI after a preDP3 under control conditions (black symbols; $n = 15$ synapses) or in the presence of latB (blue symbols; $n = 9$ synapses) or CaMip (green symbols; $n = 5$ synapses). Each size was normalized to the naive size evoked by a DP30. A double-exponential function was fitted to the time course of FRP recovery under the control condition ($\tau_{fast} = 0.06$ s and $\tau_{slow} = 3.97$ s; solid black line), and a monoexponential function was fitted to the recovery time course in the presence of latB ($\tau = 4.83$ s; solid blue line). A log-normal function, $A \cdot \exp[-(\ln(x/x_0)/\sigma)^2]$, was fitted to the change in the SRP size under control conditions or in the presence of latB (control: $x_0 = 0.19$, $A = -0.30$, $\sigma = 3.33$ s, dotted black line; latB: $x_0 = 0.16$, $A = -0.11$, $\sigma = 3.97$ s, dotted blue line). (*B, iii* and *iv*) Time courses of SRP recovery (*B, iii*) and FRP (*B, iv*) shown in an expanded scale. Averaged traces of Ca^{2+} transients evoked by a preDP3 were recorded at the calyx terminals loaded with 0.45 EGTA plus 0.05 Fura-4F and are superimposed in *B, iv* (control, green; latB, magenta; right ordinate). Error bars indicate SEM. $^*P < 0.05$; $^{**}P < 0.01$.

(100 μM), a specific myosin II inhibitor, suppressed both SDR and CDR (Fig. 2*B*, light blue). No further suppression was observed when blebbistatin was coapplied with latB via the patch pipette (Fig. 2*C*, green dots). To test whether dynamic regulation of actin filaments is necessary for SDR, we studied the effect of the actin stabilizers jasplakinolide (1 μM) and phalloidin (20 μM) and found that neither affected the recovery of the FRP when applied via the presynaptic patch pipette (Fig. 2*C*, gray and magenta symbols, respectively). Finally, we tested whether latB occludes the effects of CaMip. The effect of the coapplication of CaMip and latB was not different from that of latB alone (Fig. 2*C*, brown rectangles). These results indicate that myosin and polymerized actin filaments are required for both CDR and SDR, but dynamic reorganization of actin filaments is not required.

Recovery of Rapidly Releasing Vesicles After a Short Depolarization Occurs in Parallel with the Partial Depletion of Slowly Releasing Vesicles. We further investigated the time course of FRP and SRP recovery after a preDP3 by applying a DP30 at various ISIs. The time course of the FRP recovery showed two distinct phases: a rapid phase and a slow phase (Fig. 3*B*, *ii–iv*). The rapid phase was paralleled by a partial depletion of the SRP, which peaked at an ISI of 200 ms, suggesting that the rapid recovery of the FRP is coupled to a partial depletion of the SRP. In Fig. 3*A*, *i*, a representative trace for the quantal release rate calculated from an EPSC evoked by a DP30 200 ms after a preDP3 (red trace) is overlaid onto a control trace (black) from a single DP30. The quantal release rate was smaller during both the fast-release phase and the slow-release phase, demonstrating partial depletion of the SRP.

To test the dependence of SDR on polymerized actin, we repeated the experiments, as shown in Fig. 3*A*, *i*, in the presence of latB. In contrast to experiments without drug, the slow quantal release evoked by a DP30 was not affected substantially by a preDP3 (Fig. 3*A*, *ii*), supporting the idea that SDR is responsible for the partial depletion of the SRP. Furthermore, latB reduced both the depletion of the SRP and the amplitudes of the rapid-recovery phase of the FRP (Fig. 3*B*, *ii*). Consequently, in the presence of latB, the majority of the FRP recovered with a time course similar to that of the slow phase under control conditions.

Although we present evidence that rapid recovery of the FRP is attributable to SDR, one can argue that the size of the FRP may be overestimated at short ISIs, when residual calcium is not yet cleared. To test this possibility, we measured $[Ca^{2+}]_i$ tran-

sients induced by a preDP3 at calyx terminals. We found that $[Ca^{2+}]_i$ at an ISI of 100 ms was higher by 48 ± 3.9 nM than the resting $[Ca^{2+}]_i$ (70 ± 5.7 nM, $n = 6$; green line in Fig. 3*B*, *iv*, right ordinate). It is unlikely that a 48-nM increase in $[Ca^{2+}]_i$ had a significant effect on the estimation of the FRP size (13). Indeed, the elevation of $[Ca^{2+}]_{rest}$ by 97 ± 33 nM ($n = 5$) caused by a subthreshold depolarization (−35 mV for 250 ms) had little effect on the estimate of the FRP released by a subsequent 30-ms depolarizing pulse (Fig. S4*A*). Moreover, to test whether an elevated $[Ca^{2+}]_{rest}$ had any effect on the estimate of a partially depleted FRP size, we examined the recovered FRP size 750 ms after a preDP3, which either was or was not preceded by a subthreshold depolarization. We found that elevation of $[Ca^{2+}]_{rest}$ by *ca*. 100 nM had no effect on the recovered FRP size (Fig. S4*B*). Therefore, the rapid recovery of the FRP at ISIs longer than 100 ms cannot be attributed to residual calcium. However, the FRP estimates at ISIs <100 ms may not be reliable, because residual calcium may be very high during the kinetic phase of binding between Ca^{2+} and EGTA. Furthermore, latB, which reduced the amplitude of the rapid-recovery phase, had no effect on the amplitude of presynaptic Ca^{2+} current (Fig. 3*B*, *i*) or on the preDP3-induced $[Ca^{2+}]_i$ transients (Fig. 3*B*, *iv*; magenta line), confirming that the change in residual calcium is not relevant to the effect of latB on rapid FRP recovery. In contrast, the rapid-recovery phase persisted when CaMip was included in the presynaptic pipette, arguing against the involvement of CDR (Fig. 3*B*, green circles).

It is somewhat puzzling that a partial depletion of the SRP could be observed after a preDP3, given that the recovery of the SRP has been described as very fast, so that majority of the SRP is recovered within 100–200 ms (4). For unknown reasons, however, we found that recovery of the SRP displays a small slow phase after a preDP30 (open blue circles in Fig. S5), which was similar to the time course of SRP recovery after a preDP3 (black open symbols in Fig. S5; data taken from Fig. 3*B*, *ii*). This component may be the basis for the partial depletion of the SRP observed after a preDP3.

Roles of CDR and SDR in Short-Term Plasticity. Inhibition of CDR has been reported to reduce the sustained EPSC amplitude during high-frequency stimulation (HFS) (4, 9), but the role of reluctant SVs in short-term synaptic plasticity is not well understood. The rapid recovery of the FRP mediated by SDR (Fig. 3) implies that SDR may play a role in supplying rapidly releasing SVs during the early period of HFS before SRP vesicles are depleted. To test this hypothesis, we monitored the time course of FRP depletion during presynaptic stimulation with a train of AP-equivalent pulses (AP_es) at 100 Hz under the same experimental conditions as in Fig. 1.

Pulse protocols for monitoring the changes in the FRP size during AP_e trains are shown in Fig. 4*A*. In each protocol, an AP_e train was applied every 40 s with 1–30 AP_es followed by a 3-ms depleting test pulse (DP3). The durations of AP_e stimuli (step depolarizations from −80 mV to 0 mV) were adjusted in each synapse, such that the first EPSC amplitudes were close to 2 nA (2.35 ± 0.11 nA, 1.5–2.5 nA). This value is comparable to that evoked by a single AP in an unclamped calyx terminal in the presence of 2 mM γ-DGG (14). Examples of EPSC traces evoked by these protocols in the same synapse are superimposed in Fig. 4*B* (middle traces) together with calcium currents (top trace) and deconvolution-based release rates. The amplitudes of Ca^{2+} currents and EPSCs evoked by AP_es and DP3, respectively, are shown as a function of the stimulus number in Fig. 4 *C* and *D*. We took the FRP sizes calculated from the EPSC evoked by DP3 after a train of $n-1$ AP_es as the FRP that is available for the nth AP_e and plotted this quantity after normalization to the naive FRP size against the number of conditioning AP_es (Fig. 4*F*; henceforth such plots are referred to as "FRP depletion curves"). For all synapses

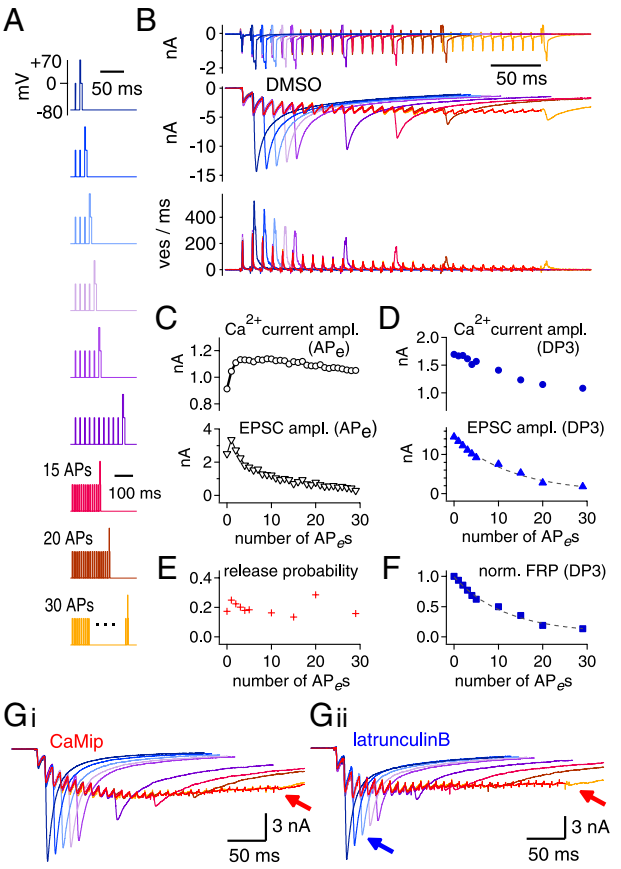

Fig. 4. Examples of experiments for monitoring FRP size during a train of AP-equivalent pulses (AP_es) at 100 Hz. (*A*) A set of voltage clamp protocols to monitor FRP size during a 100-Hz train of AP_es (HFS). After a train of various numbers (1–5, 10, 15, 20, 30) of 100-Hz AP_es (0 mV for 1.2–1.6 ms), a DP3 was applied. Each of nine pulse protocols was applied every 40 s in the same synapse. (*B*) (*Top*) Nine traces of presynaptic Ca^{2+} current ($I_{Ca,pre}$) elicited by the voltage clamp protocols shown in *A* were recorded in the same synapse and superimposed. Color codes are as in *A*. Corresponding traces of EPSCs and release rate are shown in the middle and bottom panels, respectively. The averaged traces (red) of EPSCs and quantal release rates evoked by trains of AP_es ($EPSC_{AP}$) are superimposed in the middle and bottom panels, respectively. (*C*) Amplitudes of $I_{Ca,pre}$ (*Upper*) and EPSCs (*Lower*) evoked by a train of AP_es (30 pulses at 100 Hz). (*D*) Amplitudes of $I_{Ca,pre}$ (*Upper*) and EPSCs evoked by a DP3 ($EPSC_{DP3}$) (*Lower*) as a function of AP_e numbers in the preceding train of AP_es (100 Hz). (*E* and *F*) Changes in the Pr (*E*) and the depletion time course of the FRP size (*F*) during a train of AP_es (100 Hz). See text for calculation of Pr. (*G*) Nine traces of EPSCs elicited by the voltage clamp protocols shown in *A* in the presence of CaMip (*G*, *i*) or latB (*G*, *ii*). The averaged traces of $EPSC_{AP}$ (red) are superimposed in each set of EPSC traces. Arrows indicate severe depression of $EPSC_{DP3}$ compared with control conditions.

studied, we confirmed that the naive FRP size estimated from the EPSC evoked by a DP3 was the same as that from the EPSC evoked by a DP30. Assuming that the FRP, but not the SRP, is released by an AP_e, we calculated Pr at the given nth AP_e as the $EPSC_{AP}(n)$, the amplitude of EPSC evoked by the nth AP_e, divided by the EPSC evoked by a DP3 applied after a train of $n-1$ AP_es (Fig. 4*E*).

Fig. 5*A* shows averaged traces of EPSCs evoked by AP_es ($EPSC_{AP}$) from experiments similar to those in Fig. 4 under different conditions (1/1,000 DMSO, 20 μM CaMip, or 15 μM latB in the presynaptic pipette; see Fig. 4*G* for examples of ESPC traces under the latter two conditions). The mean amplitudes of $EPSC_{AP}$ normalized to the first $EPSC_{AP}$ under the three dif-

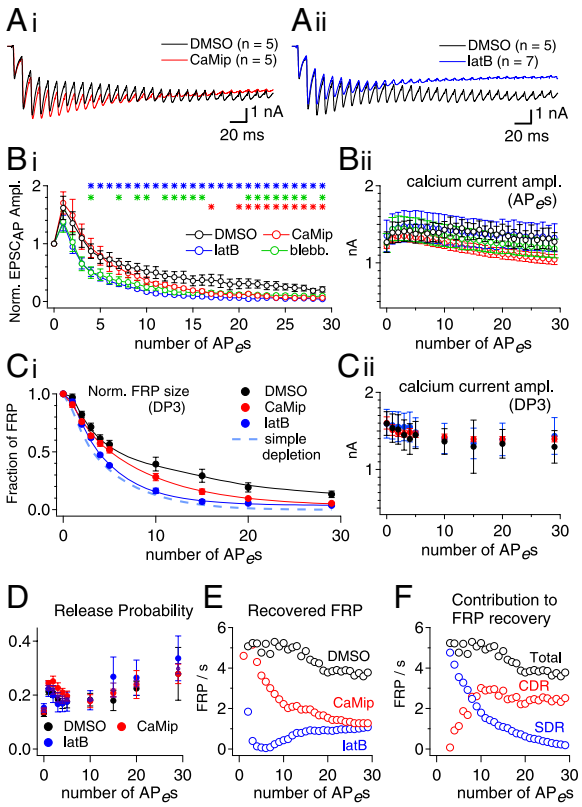

Fig. 5. SDR and CDR contribute to FRP recovery in the early and late phases of the HFS, respectively. (*A*) Averaged EPSC traces evoked by a 100-Hz train of AP$_e$s (HFS) in control conditions (black trace) and in the presence of CaMip (red trace; *A*, *i*) or latB (blue trace; *A*, *ii*) are superimposed. (*B*, *i*). Mean amplitudes of EPSCs normalized to the first EPSC amplitude as a function of AP$_e$ numbers in a 100-Hz train under control conditions (DMSO; black circles) or in the presence of CaMip (red circles), latB (blue circles), or blebbistatin (green circles). Statistical significance ($P < 0.05$) is marked by asterisks [control vs. latB (blue asterisks), blebbistatin (green asterisks), or CaMip (red asterisks). (*B*, *ii*). Amplitudes of presynaptic Ca^{2+} currents evoked by an AP$_e$ during HFS. No statistically significant differences were found in the presence of drugs as compared with the control values. (*C*, *i*) Time courses for FRP depletion during HFS. The FRP size was estimated by deconvolution of each EPSC evoked by a DP3, normalized to the naive FRP size, and plotted as a function of the preceding AP$_e$ number (DMSO, black trace; CaMip, red trace; latB, blue trace). In the presence of latB, the time course for FRP depletion during the train was most similar to that predicted by the simple depletion model (light blue broken line). (*C*, *ii*). Amplitudes of presynaptic calcium currents evoked by a DP3 as a function of the preceding AP$_e$ numbers. (*D*) Mean Pr as a function of the AP$_e$ number during HFS. (*E*) Recovery rate of the FRP during HFS in the presence of DMSO (black circles), CaMip (red circles), or latB (blue circles). (*F*) Contributions of CDR (red circles) and SDR (blue circles) to FRP recovery during HFS. The total recovery rate of the FRP (black circles) is superimposed for comparison. See text for calculation of the FRP recovery rate. Error bars indicate SEM.

ferent conditions are compared in Fig. 5*B*, *i*. Consistent with previous reports (9), CaMip reduced the sustained EPSC amplitude (red symbols; measured between the 21st and 30th EPSC; $P < 0.05$), whereas EPSC amplitudes during the early phase of the train were not influenced by CaMip. In the presence of latB (blue symbols), however, both the sustained EPSC amplitude and the early-phase EPSC amplitudes were reduced significantly (from the fifth EPSC to 30th EPSC; $P < 0.05$). The effect of blebbistatin (green circles) was similar to that of latB. The late time course of the FRP depletion under each condition (Fig. 5*C*, *i*) was similar to the corresponding decay of the EPSCs evoked by AP$_e$s under the same condition. This result indicates that the effects of CaMip and latB on the time course of EPSC$_{AP}$ can be attributed to differences in the time course of FRP depletion rather than to differences in Pr. Consistently, neither the amplitude of presynaptic Ca^{2+} current nor the Pr during the 100-Hz train was different among the three conditions (Fig. 5*B*, *ii*; *C*, *ii*; and *D*).

We tried to estimate vesicle recruitment during trains by comparing the measured FRP depletion curve with that calculated under the assumption that no recruitment occurs (broken line in Fig. 5*C*, *i*) according to the equation, $FRP_n = FRP_{n-1} \times (1 - Pr_{n-1})$. Under control conditions, the measured FRP depletion curve clearly deviated from the simple depletion curve. Inhibition of CaM caused the FRP size to be significantly lower than the control values in the late phase (15th to 30th AP$_e$; $P < 0.05$) but not during the early phase of the train, confirming the previous notion that the steady-state EPSCs during HFS are maintained through CDR (9). In contrast, latB significantly suppressed the FRP size as early as the second and subsequent AP$_e$s and thus caused the measured FRP depletion curve to be more similar to the simple depletion curve throughout the duration of the train, indicative of little FRP replenishment during the train. To quantify the contribution of CDR and SDR to FRP recovery during the AP$_e$ train, we first calculated the recovered fraction of FRP between the (n−1)th and the nth AP$_e$s (denoted by $rFRP_n$) according to the following equation: $rFRP_n = FRP_n - FRP_{n-1} \cdot (1 - Pr_{n-1})$, where FRP_n and FRP_{n-1} are the normalized FRP sizes measured at the time points of the nth and (n − 1)th AP$_e$, respectively, and Pr_{n-1} is the release probability at the (n−1)th AP$_e$. Fig. 5*E* shows the replenishment rate of the FRP during HFS, which is calculated as $rFRP_n$/10 ms, as a function of the AP$_e$ number. This analysis shows that replenishment is high, on the order of five pools/s up to about the fifth AP$_e$, for both the control and CaMip cases. Replenishment decays rapidly for CaMip afterward. We regard the differences in $rFRP_n$ values between control and CaMip conditions as CDR and the differences in $rFRP_n$ values between CaMip and latB conditions as SDR. We calculated the contributions of CDR and SDR to the FRP replenishment during HFS (Fig. 5*F*). Fig. 5*F* shows that the FRP is replenished primarily by SDR in the early phase of the train and that the contribution of CDR increases and saturates around the 10th AP$_e$, whereas SDR diminishes as the pulse number increases. The calculations also show that the FRP recovery rate during the last 10 EPSCs was 3.8 FRP/s, which is comparable to the maximal recovery rate of CDR, 3.3 FRP/s, reported by Hosoi et al. (9). These results indicate that reluctant SVs can be recruited to phasic release extremely rapidly in the early phase of HFS, before global $[Ca^{2+}]_i$ rises high enough to invoke CDR. In contrast, CDR is responsible for the sustained EPSCs in the late phase of the train.

A caveat regarding the analysis shown in Fig. 5*E* is that FRP_n may be overestimated in comparison with FRP_{n-1} because $[Ca^{2+}]_i$ is expected to rise during the stimulus train. It has been shown that 0.5 mM EGTA effectively suppresses facilitation when the FRP is largely depleted (figure 5 in ref. 15). However, residual calcium may cause a considerable error in the estimate of the FRP during the first few AP$_e$s in the train when an appreciable amount of the FRP still remains. Consequently, estimates for the recovery rate of the FRP at the first two points may not be realistic (>10 FRP/s). We therefore eliminated the first two estimates for FRP recovery from the analysis (Fig. 5 *E* and *F*).

Actin Disruption Renders the Cumulative Amplitude of EPSCs Comparable to That Evoked by a Single Long Depolarization Pulse. The RRP_{cum} is widely used to estimate the RRP size at synapses that display short-term depression because of the depletion of SVs (16). Phasic release during HFS is mediated primarily by the FRP at the calyx of Held synapse (2). Given our finding that SRP vesicles are recruited to the FRP in the early phase of a train, some of these vesicles may be included in RRP_{cum} and lead to a dis-

crepancy between this estimate and the FRP size measured from the EPSC evoked by a DP3. To test this hypothesis, we compared the amplitude of the EPSC evoked by a DP3 with the RRP_{cum} estimate from a 100-Hz train of 30 AP_e-induced EPSCs measured at the same synapse (Fig. 6). The amplitude of EPSC as estimated by RRP_{cum} was significantly larger than the amplitude of EPSC evoked by a DP3 both under control conditions (Fig. 6*A*) and in the presence of CaMip (Fig. 6*B*). When SDR was inhibited by latB, however, the amplitude estimated by RRP_{cum} was not different from the amplitude of EPSC evoked by a DP3 (Fig. 6*C*), supporting the idea that the recruitment of SVs from the SRP contributes to the phasic release and thus to the RRP_{cum} estimate.

Actin Disruption Accelerates Synaptic Depression of EPSCs Evoked by Stimulation of Afferent Fibers. To test whether SRP vesicles also are recruited to the phasic release during HFS in an unperturbed nerve terminal, we examined the effects of bath-applied latB and calmidazolium (CMZ) on the short-term plasticity of EPSCs evoked by afferent fiber stimulation with a train of 30 pulses at immature (postnatal days 7–9; Fig. 7*A*) and mature postnatal days 13–15; Fig. 7*B*) calyx of Held synapses. Although short-term depression at immature synapses is dominated by desensitization of AMPA receptors (17), cyclothiazide could not be used to prevent desensitization because of its off-target effects on ion channels in the calyx of Held under current clamp (14, 18). We examined the effects of latB and CMZ on EPSCs evoked by a 100-Hz train in the presence of 2 mM γ-DGG. Despite severe depression, probably caused by the desensitization of AMPA receptors, the effects of CMZ and latB were qualitatively similar to those observed in dual whole-cell patch conditions: LatB depressed EPSCs throughout the train, whereas CMZ depressed the sustained EPSCs (Fig. 7*A*).

The mature calyx synapse exhibits lower susceptibility to AMPA receptor desensitization (17). During maturation of the calyx of Held, the reduced Ca^{2+} influx caused by the shortening of the AP duration is compensated by the tighter spatial coupling of SVs to the calcium source (19, 20). It is puzzling, however, that the mature calyx of Held still harbors a large number of SRP vesicles (20, 21). To test whether SRP vesicles are recruited to the phasic release, we examined the effect of latB at the mature calyx synapse in the presence of 2 mM γ-DGG. The first EPSC amplitude was not affected by either CMZ or latB (Fig. 7*B*, *iii*, *Left*). However, latB, but not CMZ, induced severe depression in the early phase of the train (Fig. 7*B*, *ii*; $P < 0.05$). Accordingly,

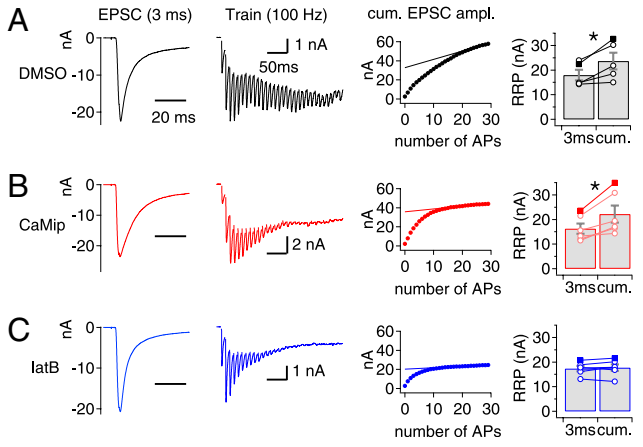

Fig. 6. Actin disruption renders the RRP estimates from an RRP_{cum} plot comparable to the amplitude of $EPSC_{DP3}$. Representative traces of EPSC evoked by a DP3 (*Left Column*) and by a train of AP_es at 100 Hz (*Second Column*) at the same synapse under control conditions (1/1,000 DMSO) (*A*) and in the presence of CaMip (*B*) or latB (*C*) in the presynaptic pipette. The RRP size was estimated from the *y*-intercept of the extrapolated line fitted to the last five points of the RRP_{cum} plot (*Third Column*). In each condition, the mean value for RRP_{cum} was compared with the amplitude of $EPSC_{DP3}$ (*Right Column*). Control, 18.00 ± 2.13 nA vs. 23.62 ± 3.38 nA, $n = 5$, $P = 0.025$; CaMip, 16.24 ± 2.09 nA vs. 22.17 ± 3.48 nA, $n = 6$, $P = 0.012$; latB, 17.38 ± 1.06 nA vs. 17.74 ± 1.33 nA, $n = 6$, $P = 0.49$; paired *t* test. Symbols connected with a line on the bar graph indicate data points measured from the same synapse. Data from representative traces are shown by filled symbols. Error bars indicate SEM. $*P < 0.05$.

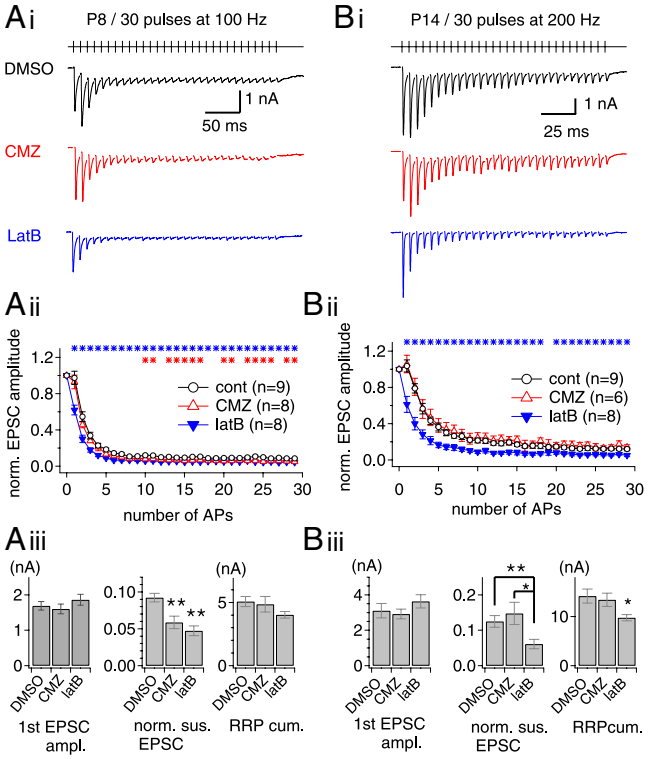

Fig. 7. Effects of actin disruption on short-term depression at the immature (postnatal days 7–9) and mature (postnatal days 13–15) calyx of Held synapses. (*A*, *i*). Representative EPSC traces evoked by stimulation of afferent axons (30 stimuli at 100 Hz) at the immature calyx of Held synapses in the presence of DMSO (vehicle; black trace), CMZ (red trace) or latB (blue trace). (*A*, *ii*) Mean values for amplitude of EPSCs normalized to the first EPSC amplitude under different conditions (control, open black circles; CMZ, open red triangles; latB, filled blue triangles). Asterisks indicate significant differences ($P < 0.05$) between control and latB (blue asterisks) or CMZ (red asterisks) conditions. (*A*, *iii*) Mean values for the first EPSC amplitude (*Left*), normalized amplitudes of the last 10 EPSCs (*Middle*), and the RRP_{cum} estimate (*Right*) under control (DMSO), CMZ, and latB conditions. (*Left*) Neither CMZ nor latB affected the baseline EPSC amplitude (DMSO, 1.69 ± 0.12 nA, $n = 9$; CMZ, 1.60 ± 0.14 nA, $n = 8$, $P = 0.62$; latB, 1.86 ± 0.15 nA, $n = 8$, $P = 0.40$). (*Center*) Normalized amplitudes of the last 10 EPSCs were reduced significantly by CMZ (DMSO, 0.092 ± 0.006; CMZ, 0.059 ± 0.008) and by latB (0.047 ± 0.007). $**P < 0.01$. (*Right*) The RRP_{cum} in the presence of latB (4.03 ± 0.26 nA) was marginally smaller than in the control condition (5.07 ± 0.40 nA) or in the presence of CMZ (4.86 ± 0.61 nA) ($P = 0.053$). (*B*, *i*) Effects of CMZ and latB on short-term plasticity of ESPCs at the mature calyx of Held synapse (postnatal days 13–15). Experimental conditions are as in *A* except for the higher stimulation frequency (200 Hz). (*B*, *ii*). Normalized amplitude of EPSCs under different conditions (control, open black circles; CMZ, open red triangles; filled blue triangles, latB). (*B*, *iii*) In the first EPSC amplitude, no significant difference was found between the three conditions (DMSO, 3.11 ± 0.40 nA, $n = 9$; CMZ, 2.92 ± 0.27 nA, $n = 6$, $P = 0.74$; latB, 3.63 ± 0.37 nA, $n = 8$, $P = 0.36$). The sustained EPSC amplitude was reduced significantly by latB (DMSO, 0.13 ± 0.02; latB, 0.06 ± 0.01) but not by CMZ (0.15 ± 0.03; $P = 0.50$). The RRP_{cum} was reduced significantly by latB (DMSO, 14.14 ± 1.42 nA; latB, 9.75 ± 0.65 nA; $P = 0.017$) but not by CMZ (13.40 ± 1.34 nA, $P = 0.73$). Error bars indicate SEM. $*P < 0.05$; $**P < 0.01$.

the mean RRP_{cum} estimate in the presence of latB was significantly lower than the control value (Fig. 7*B*, *iii*, *Right*). In light of our finding that SDR depends on polymerized actin in the immature calyx of Held, SRP vesicles also may be recruited rapidly to the phasic release in the mature calyx terminals. Interestingly, in the presence of CMZ, the mean value for the last 10 normalized EPSCs was not different from the control value (Fig. 7*B*, *iii*, *Center*), suggesting that CDR may not be activated by a 200-Hz train in the mature calyx terminal.

SDR Facilitates the Recovery of the EPSC After a Short Burst. Previously, it was demonstrated at immature calyx synapses that EPSCs recover with a single, slow exponential time course after mild stimulation (11 APs at 100 Hz) of afferent fibers, whereas a fast-recovery phase emerged after stronger stimulation (30 APs at 300 Hz) (22). One can argue that the single-component slow recovery after mild stimulation is not consistent with our finding of rapid recovery of the FRP after a preDP3 (Fig. 3*B*). However, SDR decays rapidly during a 100-Hz train (to 30% of its initial peak at the 11th pulse; Fig. 5*F*). It therefore is expected that SDR contributes little to the recovery of the EPSC after a 100-Hz train of 11 APs (22). Furthermore, $[Ca^{2+}]$ rapidly returns to the baseline after the train, so CDR contributes little to the recovery. For these reasons, one would expect fast recovery both for shorter trains (when the SRP is not yet depleted) and for longer trains (when CDR sets in). The slow recovery of EPSCs after the 100-Hz train of 11 APs in the previous report (22) may indicate that neither CDR nor SDR contributes significantly at an intermediate number of APs.

It was not feasible to test this scenario at an immature calyx of Held synapse because receptor desensitization could not be blocked pharmacologically at an intact terminal (see the legend of Fig. 7 and the discussion thereof). Instead, we studied the time course of EPSC recovery in a mature (postnatal day 14) calyx of Held synapse, which exhibits little AMPA receptor desensitization and lacks CDR as probed with a 200-Hz train (Fig. 7*B*). We compared the recovery time courses of EPSCs after stimulation of afferent fibers with a 200-Hz train of either seven or 15 pulses, whereby different amounts of the SRP would be expected to be depleted. The larger residual SRP would result in the larger fast-recovery phase. Indeed, the fast-recovery phase was evident after a train of seven pulses but not after a train of 15 pulses (Fig. 8*A*, *Inset*). Furthermore, pretreatment with latB suppressed the fast-recovery phase after the seven-pulse train (Fig. 8*C*) but had no appreciable effect on the recovery after the 15-pulse train (Fig. 8*D*). As a result, the EPSC recovery after the 7-pulse train became little different from that after the 11-pulse train in the presence of latB (Fig. 8*B*, *Inset*). Given that CDR is absent in this synapse at 200 Hz (Fig. 7*B*), the fast-recovery phase after the seven-pulse train can be attributed to SDR. Therefore, we conclude that SDR facilitates the recovery of EPSCs after a short burst of APs.

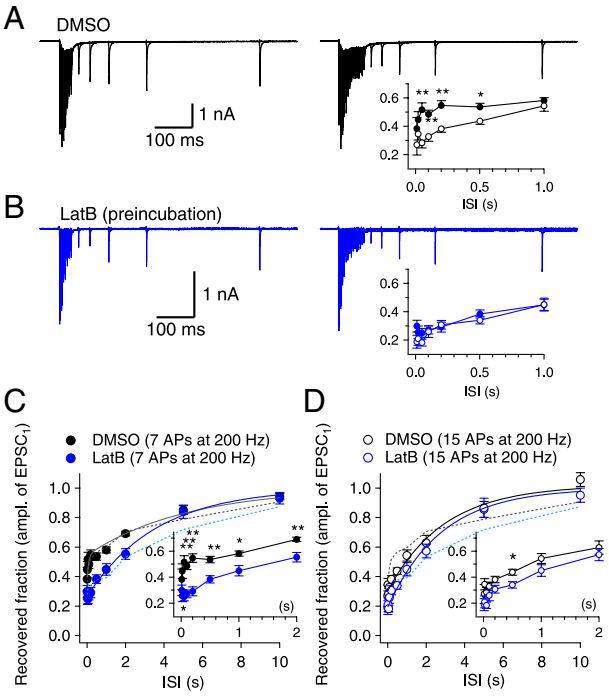

Fig. 8. SDR facilitates the recovery of the EPSC after a short burst in a mature calyx of Held synapse. (*A*) Recovery of the EPSC after a 200-Hz train of seven or 15 pulses at the same synapse. (*B*) Similar experiments in a calyx synapse pretreated with 15 μM latB for 30 min. (*Insets*) Time courses of EPSC recovery after a train of seven pulses (filled circles) and after a train of 15 pulses (open circles). (*C*) Time courses of EPSC recovery after a train of seven pulses at 200 Hz under control conditions (black circles; $n = 7$) and in the presence of latB (blue circles; $n = 6$); the curves were fitted with a biexponential function (dark gray line, $\tau_{fast} = 83$ ms, $\tau_{slow} = 5.14$ s; control) and a monoexponential function (blue line, $\tau = 3.36$ s; latB), respectively. (*D*) Recovery of the EPSC after a train of 15 pulses (control, black circles, $n = 7$; latB, blue circles, $n = 6$). Both curves were fitted with a monoexponential function ($\tau = 2.92$ s, control; $\tau = 2.81$, latB). The time courses for FRP recovery after a preDP3 (dotted lines) are superimposed for comparison (data from Fig. 3*B*, *ii*). *Insets* in *C* and *D* show time courses for EPSC recovery in an expanded time axis. $*P < 0.05$; $**P < 0.01$.

Discussion

The role of reluctantly releasing vesicles in short-term plasticity has not been recognized other than for asynchronous release (2). Based on the finding that these vesicles are very similar in their intrinsic Ca^{2+} sensitivity to vesicles contributing to synchronous release (5), positional priming has been proposed as a mechanism for the interconversion between the two types of vesicle (7). We have presented evidence supporting this hypothesis by demonstrating a posttetanic increase in the ratio of fast to slowly releasing vesicles while the total RRP remained constant (8). In the present study, using conditioning depolarizations of various durations, which caused the full depletion of the FRP and partial depletion of the SRP, we show that the recovery of the FRP can be accelerated by vesicles remaining in the SRP (Fig. 1). This idea is supported by the observation that the fast-recovery phase of the FRP after its depletion is accompanied by a partial depletion of the SRP (Fig. 3). Actin disruption suppressed not only the fast-recovery phase of the FRP size but also a concomitant depletion of the SRP. Based on these results, we conclude that SRP vesicles can be recruited to the FRP by an actin-dependent mechanism, SDR, and that this mechanism mediates the rapid-recovery phase of the FRP.

Previously, we have shown that the posttetanic change in the FRP/SRP ratio is mediated by the CaM-dependent activation of MLCK. Such a change in the FRP/SRP ratio could be observed when recombinant CaM was included in the presynaptic pipette (8). The MLCK effect should be differentiated from CDR because CDR does not shift the equilibrium but accelerates the recovery toward the previous equilibrium, whereas activation of MLCK causes a shift of the equilibrium in the sizes of the FRP and SRP. Furthermore, the present study was performed without CaM included in the presynaptic pipette, and thus no shift of equilibrium was observed after a preDP30 which induces CDR.

Functional Role of Actin in Presynaptic Terminals. Actin is colocalized with the active zone marker, bassoon (23). Given that actin constitutes a component of the active zone (AZ), the inhibitory effects of actin disruption on CDR and SDR suggest that both recruitment mechanisms may require an intact cytomatrix at the AZ. Fusion of SVs and consequent added vesicle membrane can result in disorganization of the AZ (24), which

may compromise the positional and/or molecular priming of the remaining SRP vesicles. The inhibition of CDR and SDR by actin-specific agents can be explained in light of the idea that polymerized actin facilitates the restoration of the disorganized AZ, either through release-site clearance (25) or more generally in maintaining an intact ultrastructure.

As an alternative possibility, the actin network may serve as a track for lateral movements of SVs and/or Ca^{2+} channels at an AZ. It has been found recently that at photoreceptor ribbon synapses presynaptic Ca^{2+} channels are mobile in a confinement domain, probably an AZ (26). Furthermore, actin disruption enlarges such domains and abolishes their movements associated with stimulation (26). No study is available that visualizes similar movements of SVs at the subplasmalemmal region of a presynaptic terminal. In neuroendocrine cells, cortical actin has the role of a trail that allows subplasmalemmal movement of large, dense core vesicles (27). Slowly releasing granules undergo greater lateral translocation before the fusion event than do rapidly releasing or nonfusing secretory granules during cholinergic stimulation in chromaffin cells (28). These results, together with the existence of a subplasmalemmal actin network in presynaptic terminals, imply that SVs in the subplasmalemmal region might be mobile in the nano-scale range (29).

Molecular vs. Positional Priming as a Mechanism for SRP-Dependent Recovery. There is a debate about whether the primary factor determining whether a docked SV is slow or fast is its proximity to the Ca^{2+} source or its intrinsic Ca^{2+} sensitivity for fusion. These alternatives are referred to as the "positional priming" and "molecular priming" hypotheses, respectively (6, 7). We interpreted the involvement of actin and myosin in SDR as evidence supporting the positional priming hypothesis as a mechanism for SDR. However, our results do not exclude the molecular priming hypothesis, because actin filaments also may serve as a chemical scaffold to increase the local concentration of molecules, which influence the Ca^{2+} sensitivity of SVs and thereby catalyze the transformation of SVs from SRP into FRP (30).

About one half of release-competent SVs exhibit a fast-release rate after periods of rest, and thus far only two kinds of signaling are known to alter the ratio of the size of the FRP to the size of the SRP (8, 31), suggesting that the steady-state ratio is maintained quite robustly. Given that the specific depletion of the FRP triggers the conversion of slow SVs into fast SVs (SDR), it is reasonable to assume that a limited resource is necessary for the conversion. In view of the positional priming hypothesis, we think that calcium channels are the best candidates for this resource regulating the size of the FRP (7). Alternatively, to explain SDR in the light of the molecular priming hypothesis, a molecule (or molecules) required for the final step of molecular maturation of a docked SV should be postulated, and this molecule should be present in limited amounts. The identification of such a molecule certainly would advance the molecular priming hypothesis.

Although slow vesicles are released much faster by homogeneous Ca^{2+} elevation using flash photolysis than by a depolarizing pulse, the intrinsic Ca^{2+} sensitivity of slow-releasing SVs still was slightly lower than that of fast-releasing SVs (5). Additionally, slowing of the fast-release time constant of EPSCs has been reported after partial depletion of FRP using low-frequency stimulation of the calyx of Held (32). Consistent with these previous findings, we noted that the fast-release time constant of the second EPSC after a preDP3 was ~1.5 times slower than that of the first EPSC. These findings suggest that SVs newly recruited through SDR may be immature in regards to their molecular priming. Such kinetic aspects and their influence on Pr need further consideration.

SRP-Dependent Recovery vs. Asynchronous Release of Reluctant SVs at Glutamatergic Synapses. Our results, together with a previous report (2), show that SRP vesicles either can be asynchronously released or can be recruited into the FRP, contributing to the phasic release during HFS. The higher buildup of global $[Ca^{2+}]$ will cause greater asynchronous release of SRP vesicles (33) and thus will reduce the number of SRP vesicles available for SDR. This idea is consistent with the previous finding that asynchronous release and phasic release compete for a common, limited supply of release-competent SVs (34). Therefore, the fate of SRP vesicles—conversion to FRP vesicles or asynchronous release—may be determined by presynaptic global $[Ca^{2+}]_i$. Keeping global $[Ca^{2+}]$ low during HFS at presynaptic terminals not only will reduce asynchronous release but also will ensure a rapid supply of SVs from the SRP to the FRP, enhancing phasic release. Compared with the immature calyx of Held, the mature one exhibits more efficient Ca^{2+} clearance mechanisms (35, 36) and requires less Ca^{2+} influx for neurotransmission because of nanodomain coupling (20). These developmental changes may optimize the mature calyx terminal for SDR while minimizing asynchronous release.

Physiological Implications of SRP-Dependent Recovery at the Mature Calyx of Held. Whether mature calyx terminals lack the mechanism of CDR remains to be elucidated. The lower build-up of global $[Ca^{2+}]$ during high-frequency activity at the mature calyx of Held may be one of the reasons why calmidazolium had little effect on the sustained amplitude of EPSCs during 200-Hz trains (Fig. 7*B*). The reduced contribution of CDR at the mature calyx is in line with previous findings regarding a developmental decrease in the Ca^{2+}-dependent modulation of presynaptic Ca^{2+} channels (19, 37) and short-term plasticity (38, 39). Given that full depletion of the SRP is unlikely under physiological conditions in vivo (38), the SRP may play an important role in supplying SVs to the FRP and thus may be responsible for the reduced short-term depression observed in the mature calyx of Held synapse (38). Therefore, SDR may be essential for maintaining the background EPSC amplitude under in vivo conditions, when the calyx is invaded constantly by low-frequency APs. However, it is still possible that CDR may play a role in the recovery after or during prolonged sound stimulation that transiently increases the AP frequency to several hundred Hertz.

Materials and Methods

Brain Slice Preparation and Electrophysiology. Transverse brainstem slices (200 μm thick) containing the medial nucleus of trapezoid body (MNTB) were prepared from 7- to 9-d-old Sprague–Dawley rats. Protocols were approved by the Animal Care Committee of Seoul National University. Brains were chilled in ice-cold low-calcium aCSF. Slices were made using a vibratome slicer (VT1200; Leica), and were incubated at 37 °C for 30 min in normal aCSF and thereafter were maintained at room temperature (23–25 °C) until required. The low-calcium aCSF contained (in mM) 125 NaCl, 25 $NaHCO_3$, 2.5 KCl, 1.25 NaH_2PO_4, 2.5 $MgCl_2$, 0.5 $CaCl_2$, 25 glucose, 0.4 Na ascorbate, 3 myoinositol, and 2 Na pyruvate [pH 7.4 when saturated with carbogen (95% O_2, 5% CO_2); osmolarity, ~320 mOsm]. The constituents of normal aCSF were the same as low-calcium aCSF except for 1 mM $MgCl_2$ and 2 mM $CaCl_2$. Slices were transferred to a recording chamber in an upright microscope (BX50WI; Olympus). In most experiments (except in Fig. 7), 1 μM tetrodotoxin (TTX), 50 μM D-2-amino-5-phosphonovaleric acid (D-AP5), and 10 mM tetraethylammonium chloride (TEA-Cl) were added to the normal aCSF to isolate the presynaptic Ca^{2+} current and AMPA receptor-mediated EPSC. Also, 100 μM cyclothiazide and 2 mM γ-DGG I (a low-affinity AMPA receptor antagonist) were added to prevent desensitization and saturation of AMPA receptors, respectively. The addition of 2 mM γ-DGG reduced the EPSC amplitude to a half of the control value. A presynaptic terminal and the postsynaptic MNTB neurons were whole-cell clamped simultaneously at −80 mV and −70 mV, respectively. The postsynaptic pipette solution (2–3 MΩ) contained (in mM) 130 Cs-gluconate, 20 TEA-Cl, 10 NaCl, 20 Hepes, 5 Na-phosphocreatine, 4 Mg-ATP, and 10 EGTA with pH adjusted at 7.3. The presynaptic patch pipette solution (3–4 MΩ) contained (in mM) 130 Cs-gluconate, 20 TEA-Cl, 20 Hepes, 5 Na-phosphocreatine, 4 Mg-ATP, 0.3 Na-GTP, and 0.5 EGTA with pH adjusted to 7.3 using CsOH. The presynaptic series resistance (R_S; 10–25 MΩ) was compensated by 50–80%, and the postsynaptic R_S (4–15 MΩ) was compensated by up to 70%, so that remaining uncompensated R_S values are

5 MΩ and 3–4 MΩ for pre- and postsynaptic pipettes, respectively. The remaining postsynaptic resistance was compensated further off-line. To obtain a square-like presynaptic calcium current, a preDP or a depleting pulse (DP) was used, comprised of depolarization to 0 mV preceded by predepolarization to +70 mV for 2 ms (Fig. 1*A*). The duration of preDP or DP was defined by the duration of the 0-mV step. In the experiment shown in Fig. 7, EPSCs were evoked by stimulating presynaptic axons (100–200 μs duration; 10–20 V intensity) with a bipolar stimulating electrode (TM53CCINSl; World Precision Instruments) placed at the midline of the brainstem in the presence of 2 mM γ-DGG and 0.1 mM picrotoxin. Stimulation was generated by a Master-8 (A.P.I.). The whole-cell recordings were made using an EPC10/2 amplifier (HEKA) at room temperature (23–25 °C). TTX, DL-AP5, cyclothiazide, γ-DGG, and dynasore were purchased from Tocris. Calmodulin inhibitory peptide, jasplakinolide, latrunculin B, and calmidazolium were obtained from Calbiochem. Blebbistatin and phalloidin were obtained from Biomol. Fura-4F was purchased from Molecular Probes. All other chemicals were obtained from Sigma. Lipid-soluble drugs were dissolved with a final DMSO concentration of 1/1,000 (vol/vol). The same amount of DMSO was added for the control conditions. We confirmed that these drugs had little effect on the baseline EPSC parameters compared with their vehicle (DMSO) (Fig. S6).

In the experiment for Fig. 3*B*, *iv*, to measure presynaptic $[Ca^{2+}]_i$, 0.5 mM EGTA in the presynaptic pipette solution was replaced with 0.45 mM EGTA and 0.05 mM Fura-4F. The excitation light from a monochromator (Polychrome-IV; TILL Photonics) was delivered to the upright microscope via a quartz light guide and a built-in condenser. Imaging was performed using a 60× water-immersion objective (NA, 0.9; LUMPlanFl; Olympus) and an air-cooled slow-scan CCD camera (SensiCAM; PCO). We used the built-in on-chip binning function (8 × 16 pixels) to accelerate the frame rate (40 Hz at the exposure time of 5 ms).

Deconvolution Method. Quantal release rates were estimated with the deconvolution method which corrects the delayed glutamate clearance component of synaptic cleft at the calyx of Held synapse (40) (http://www.mpibpc.mpg.de/groups/neher). Using the fitting protocol, we determined the parameters of the glutamate diffusion model at the start of each experiment. The criteria for an appropriate parameter set were as follows: (*i*) Residual current was small or absent after the first pulse of the fitting protocol. (*ii*) No negative release rate occurred during a whole trace. (*iii*) After stimulation, no transmitter release was expected, and the release rate should have been zero between stimulation episodes. After determining the parameters for a given synapse, we used the same parameters for other traces within the same cell pair. Cumulative release was obtained from the integration of release rate traces without correction of presynaptic vesicle replenishment and fitted with a double-exponential function. Cumulative release traces were fitted from the onset of release to 5 ms after the end of pulse, and we checked whether the total pool size obtained from the fitting was approximately the same as the total pool size that was read out manually at the end of the pulse. When slow releases continued after a 30-ms depolarization, the steady-state value of the fitting function was constrained at the cumulative release which was read out manually 15 ms after the end of the pulse. The pool size and the release time constant of two components (FRP and SRP) were obtained from the fitting. We regarded the FRP as a faster component of the biexponential fit to a cumulative release. In the dual-pulse protocol, the second pulse was fitted with a biexponential function by allowing for two time constants as free parameters because we could not obtain the best fit when the time constants were fixed at the same values as used for the first pulse, especially when the fast time constant was not fully recovered at a short ISI after a preDP3 or a preDP10.

Data Analysis. Data were analyzed using IgorPro version 6.0 (WaveMetrics). Statistical data are expressed as the mean ± SEM, and n indicates the number of synapses studied. Statistical analyses on data obtained from the same synapse and those on data from different synapses were performed using Student's paired t test and the Student's t test, respectively. For simplicity, some data with no statistically significant differences are not shown in the text.

ACKNOWLEDGMENTS. We thank Dr. E. Neher and Dr. R. Schneggenburger for critical reading of this manuscript and invaluable comments. This research was supported by Brain Research Center Grant 2009K001247 and bioMembrane Plasticity Research Center Grant 2010-0029396. J.S.L. is a postgraduate student supported by Program BK21.

1. Moulder KL, Mennerick S (2005) Reluctant vesicles contribute to the total readily releasable pool in glutamatergic hippocampal neurons. *J Neurosci* 25:3842–3850.
2. Sakaba T (2006) Roles of the fast-releasing and the slowly releasing vesicles in synaptic transmission at the calyx of held. *J Neurosci* 26:5863–5871.
3. Stevens CF, Williams JH (2007) Discharge of the readily releasable pool with action potentials at hippocampal synapses. *J Neurophysiol* 98:3221–3229.
4. Sakaba T, Neher E (2001) Calmodulin mediates rapid recruitment of fast-releasing synaptic vesicles at a calyx-type synapse. *Neuron* 32:1119–1131.
5. Wadel K, Neher E, Sakaba T (2007) The coupling between synaptic vesicles and Ca2+ channels determines fast neurotransmitter release. *Neuron* 53:563–575.
6. Wölfel M, Lou X, Schneggenburger R (2007) A mechanism intrinsic to the vesicle fusion machinery determines fast and slow transmitter release at a large CNS synapse. *J Neurosci* 27:3198–3210.
7. Neher E, Sakaba T (2008) Multiple roles of calcium ions in the regulation of neurotransmitter release. *Neuron* 59:861–872.
8. Lee JS, Ho WK, Lee SH (2010) Post-tetanic increase in the fast-releasing synaptic vesicle pool at the expense of the slowly releasing pool. *J Gen Physiol* 136:259–272.
9. Hosoi N, Sakaba T, Neher E (2007) Quantitative analysis of calcium-dependent vesicle recruitment and its functional role at the calyx of Held synapse. *J Neurosci* 27: 14286–14298.
10. Perkins GA, et al. (2010) The micro-architecture of mitochondria at active zones: Electron tomography reveals novel anchoring scaffolds and cristae structured for high-rate metabolism. *J Neurosci* 30:1015–1026.
11. Saitoh N, Hori T, Takahashi T (2001) Activation of the epsilon isoform of protein kinase C in the mammalian nerve terminal. *Proc Natl Acad Sci USA* 98:14017–14021.
12. Sakaba T, Neher E (2003) Involvement of actin polymerization in vesicle recruitment at the calyx of Held synapse. *J Neurosci* 23:837–846.
13. Felmy F, Neher E, Schneggenburger R (2003) Probing the intracellular calcium sensitivity of transmitter release during synaptic facilitation. *Neuron* 37:801–811.
14. Lee JS, Kim M-H, Ho W-K, Lee S-H (2008) Presynaptic release probability and readily releasable pool size are regulated by two independent mechanisms during posttetanic potentiation at the calyx of Held synapse. *J Neurosci* 28:7945–7953.
15. Sakaba T, Neher E (2001) Quantitative relationship between transmitter release and calcium current at the calyx of held synapse. *J Neurosci* 21:462–476.
16. Schneggenburger R, Sakaba T, Neher E (2002) Vesicle pools and short-term synaptic depression: Lessons from a large synapse. *Trends Neurosci* 25:206–212.
17. Taschenberger H, Scheuss V, Neher E (2005) Release kinetics, quantal parameters and their modulation during short-term depression at a developing synapse in the rat CNS. *J Physiol* 568:513–537.
18. Ishikawa T, Takahashi T (2001) Mechanisms underlying presynaptic facilitatory effect of cyclothiazide at the calyx of Held of juvenile rats. *J Physiol* 533:423–431.
19. Taschenberger H, Leão RM, Rowland KC, Spirou GA, von Gersdorff H (2002) Optimizing synaptic architecture and efficiency for high-frequency transmission. *Neuron* 36:1127–1143.
20. Wang LY, Neher E, Taschenberger H (2008) Synaptic vesicles in mature calyx of Held synapses sense higher nanodomain calcium concentrations during action potential-evoked glutamate release. *J Neurosci* 28:14450–14458.
21. Kochubey O, Han Y, Schneggenburger R (2009) Developmental regulation of the intracellular Ca2+ sensitivity of vesicle fusion and Ca2+-secretion coupling at the rat calyx of Held. *J Physiol* 587:3009–3023.
22. Wang L-Y, Kaczmarek LK (1998) High-frequency firing helps replenish the readily releasable pool of synaptic vesicles. *Nature* 394:384–388.
23. Morales M, Colicos MA, Goda Y (2000) Actin-dependent regulation of neurotransmitter release at central synapses. *Neuron* 27:539–550.
24. Ceccarelli B, Grohovaz F, Hurlbut WP (1979) Freeze-fracture studies of frog neuromuscular junctions during intense release of neurotransmitter. I. Effects of black widow spider venom and Ca2+-free solutions on the structure of the active zone. *J Cell Biol* 81:163–177.
25. Hosoi N, Holt M, Sakaba T (2009) Calcium dependence of exo- and endocytotic coupling at a glutamatergic synapse. *Neuron* 63:216–229.
26. Mercer AJ, Chen M, Thoreson WB (2011) Lateral mobility of presynaptic L-type calcium channels at photoreceptor ribbon synapses. *J Neurosci* 31:4397–4406.
27. Lang T, et al. (2000) Role of actin cortex in the subplasmalemmal transport of secretory granules in PC-12 cells. *Biophys J* 78:2863–2877.
28. Degtyar VE, Allersma MW, Axelrod D, Holz RW (2007) Increased motion and travel, rather than stable docking, characterize the last moments before secretory granule fusion. *Proc Natl Acad Sci USA* 104:15929–15934.
29. Gotow T, Miyaguchi K, Hashimoto PH (1991) Cytoplasmic architecture of the axon terminal: Filamentous strands specifically associated with synaptic vesicles. *Neuroscience* 40:587–598.
30. Sankaranarayanan S, Atluri PP, Ryan TA (2003) Actin has a molecular scaffolding, not propulsive, role in presynaptic function. *Nat Neurosci* 6:127–135.
31. Sakaba T, Neher E (2001) Preferential potentiation of fast-releasing synaptic vesicles by cAMP at the calyx of Held. *Proc Natl Acad Sci USA* 98:331–336.
32. Müller M, Goutman JD, Kochubey O, Schneggenburger R (2010) Interaction between facilitation and depression at a large CNS synapse reveals mechanisms of short-term plasticity. *J Neurosci* 30:2007–2016.
33. Chang CY, Mennerick S (2010) Dynamic modulation of phasic and asynchronous glutamate release in hippocampal synapses. *J Neurophysiol* 103:392–401.
34. Otsu Y, et al. (2004) Competition between phasic and asynchronous release for recovered synaptic vesicles at developing hippocampal autaptic synapses. *J Neurosci* 24:420–433.

35. Felmy F, Schneggenburger R (2004) Developmental expression of the Ca2+-binding proteins calretinin and parvalbumin at the calyx of held of rats and mice. *Eur J Neurosci* 20:1473–1482.
36. Müller M, Felmy F, Schwaller B, Schneggenburger R (2007) Parvalbumin is a mobile presynaptic Ca2+ buffer in the calyx of held that accelerates the decay of Ca2+ and short-term facilitation. *J Neurosci* 27:2261–2271.
37. Nakamura T, Yamashita T, Saitoh N, Takahashi T (2008) Developmental changes in calcium/calmodulin-dependent inactivation of calcium currents at the rat calyx of Held. *J Physiol* 586:2253–2261.
38. Crins TT, Rusu SI, Rodríguez-Contreras A, Borst JG (2011) Developmental changes in short-term plasticity at the rat calyx of Held synapse. *J Neurosci* 31:11706–11717.
39. Korogod N, Lou X, Schneggenburger R (2005) Presynaptic Ca2+ requirements and developmental regulation of posttetanic potentiation at the calyx of Held. *J Neurosci* 25:5127–5137.
40. Neher E, Sakaba T (2001) Combining deconvolution and noise analysis for the estimation of transmitter release rates at the calyx of held. *J Neurosci* 21: 444–461.